

# Experimental assessment of confined masonry walls retrofitted with SRG under lateral cyclic loads

Jhair Yacila<sup>a,\*</sup>, Jhoselyn Salsavilca<sup>a</sup>, Nicola Tarque<sup>a</sup>, Guido Camata<sup>b</sup>

<sup>a</sup>*Pontifical Catholic University of Peru, Civil Engineering Division, Lima, Peru*

<sup>b</sup>*Università degli Studi Gabriele D'Annunzio, Department of Engineering and Geology, Pescara, Italy*

---

## Abstract

Around the world, many informal masonry buildings have collapsed due to the failure of their bearing walls under lateral seismic loads. This is related to the many involved factors, such the quality of the materials, the quality of workmanship, the lack of technical intervention, and the high seismicity of the zone, among others. However, the fact is that these constructions need to be retrofitted in order to upgrade their ultimate strength and allow them to properly absorb inelastic deformations. Currently, fiber reinforced polymer (FRP) has been widely studied as a retrofitting technique. However, it has some technical and economic disadvantages that are remedied by fiber reinforced mortar (FRM). In this paper, a variant of FRM known as steel reinforced grout (SRG) is studied as a seismic retrofitting technique for cracked confined masonry walls (CMW). For this purpose, three full-scale cracked walls were repaired, retrofitted with SRG strips, and tested under in-plane cyclic loads at the Pontifical Catholic University of Peru (PUCP). The experimental results show the benefits of SRG in improving the lateral displacement ductility, energy dissipation, and stiffness degradation of CMWs.

*Keywords:* confined masonry wall, seismic retrofit, SRG, seismic vulnerability

---

## 1. Introduction

Confined masonry is a type of construction widely diffused in Peru due to its easy and fast construction. According to [1], masonry dwellings represent 84% of the total

---

\*Corresponding author

*Email address:* jhair.yacila@pucp.edu.pe (Jhair Yacila)

buildings in Peru and 60% of them were built informally. In the case of informal  
5 dwellings, seismic events have evidenced their high vulnerability, which has led to  
human and material loss (i.e. Lima, 1746; Arequipa, 2001; Pisco, 2007). Therefore,  
there is a necessity to reinforce a huge quantity of confined masonry buildings in order  
to improve their seismic performance.

The main aim of seismic retrofitting is to upgrade the ultimate strength of the build-  
10 ing by improving the structure's ability to absorb inelastic deformations [2]. In this  
way, external reinforcement by using composite materials has arisen as an efficient  
method due to its advantages, such as its facility of application, high stress/weight ra-  
tio, and versatility, which means it is applicable to different types of substrates. In  
this way, one of the most commercial composites is the well-known fiber reinforced  
15 polymer (FRP). This composite consists of different kinds of fibers (e.g. carbon, glass,  
basalt, and others), or high strength textiles and an organic binder (e.g. epoxy resin).  
Different studies have been conducted to assess the effectiveness of the FRP when  
retrofitting masonry walls. For instance, [2, 3, 4] demonstrated that FRP can signifi-  
cantly increase the strength, ductility and energy absorption capacity of the masonry  
20 walls. In addition, FRP are cataloged as convenient because it does not add mass to  
the structure, it is easy to handle, flexible, quick to install, and have an excellent per-  
formance in terms of tensile strength and durability [5, 6]. Nevertheless, FRP has also  
some disadvantages which are related to its inapplicability on wet surfaces, its poor  
performance at high temperatures and in alkaline environments, possible hazards for  
25 workers, the incompatibility of the resin with the substrate materials, and the lack of  
water vapor permeability [7, 8, 9]. On the other hand, reinforcement systems based  
on cement (fiber reinforced cementitious matrix, FRCM) and mortar (fiber reinforced  
mortar, FRM, or textile reinforced mortar, TRM), have arisen to overcome these draw-  
backs. Furthermore, they are reversible (i.e. they can be removed from the surface  
30 without major damage) and are not architecturally invasive since the thickness of the  
intervention can be 10 mm or less.

A TRM composite can comprise different types of fiber: basalt, glass, carbon,  
polyparaphenylene benzobisoxazole (PBO), aramid, among others. A particular case  
of TRM is given when the steel fiber or textile is used into the composite because it

35 is more commonly known as steel reinforced grout (SRG), which has already been  
experimentally studied as a retrofitting technique for concrete and masonry structures  
[10, 11, 12]. This composite is of great interest due to its mechanical properties and  
bond efficiency. For instance, steel fibers have a high tensile strength, a higher stiffness  
than basalt or glass, and less thickness than carbon and aramid. These particular fibers  
40 are less fragile than the others because a ductile behaviour is exhibited before tensile  
failure. Furthermore, due to the zinc coating, steel textiles do not get rusty and are  
protected from sulphate attacks [13]. However, their application is recent compared to  
other fibers. Hence, knowledge about their design, construction and modeling is still  
limited.

45 Regarding the application of SRG as retrofitting technique of confined masonry  
walls, it has not yet been studied, which represents a gap in the search of economic  
alternatives which can help to reduce the seismic vulnerability of confined masonry  
buildings. This paper presents a criterion for designing, as well as the application  
process for retrofitting, confined masonry walls with SRG to support in-plane shear  
50 loads. Hopefully this will contribute to the formation of guidelines for their design and  
application. For the design process, the CNR and AC434 guidelines have been taken  
into account [14, 15]. Although the CNR guideline is focused on FRP, it has been  
assumed that it is also applicable to SRG since similar design concepts were applied.  
The construction process for retrofitting confined masonry walls with SRG, as well  
55 as the considerations to be taken into account during the experimental campaign, are  
also discussed. The experimental results are presented and discussed in terms of lateral  
deformation, energy dissipation, hysteresis damping, and stiffness degradation.

## 2. Previous Work

### 2.1. Description of the tested walls

60 In the experimental campaign conducted by [16, 17], a total of 9 full-scale confined  
masonry walls were built and tested under cyclic lateral loads at the PUCP. These walls  
were built with *king kong* bricks of 18 holes with a net area less than 60% of the  
gross area. These are industrial bricks, with dimensions 230 x 130 x 90 mm, and are

commonly used for bearing walls in Peru, although prohibited by the Peruvian Seismic  
 65 Code in the coastal area [18]. The construction process of a typical confined masonry  
 wall implies that steel reinforcing is located in its final position before constructing  
 the masonry panel. It is not recommended to lay the bricks more than 1.3 m high  
 per working day, in order to avoid crushing the mortar in the lower part of the panel.  
 The typical mortar thickness, either horizontal or vertical, varies between 10 and 15  
 70 mm and has a typical volumetric ratio cement/sand of 1/4. Moreover, an intentional  
 toothed finish is left for a subsequent concrete casting. In this way, it is intended to  
 guarantee a monolithic union between concrete and masonry. The dimensions of a  
 typical confined masonry wall as well as the reinforcing detail are shown in Fig. 1.

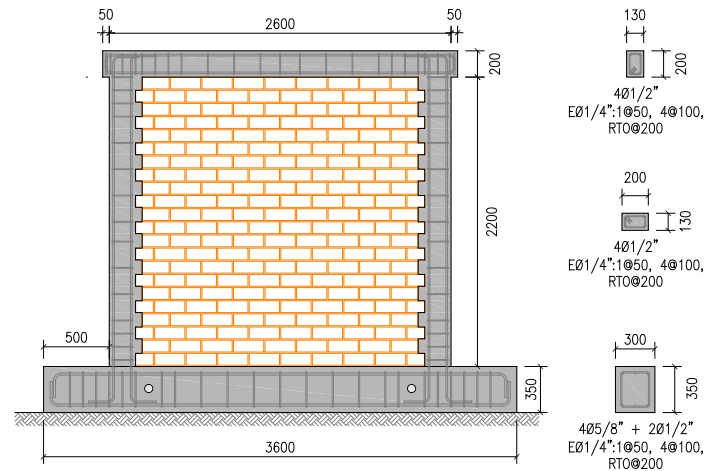


Figure 1: Geometry and reinforcement detail of a typical wall (dimensions in millimeters)

Regarding the detail of reinforcement of the confining frames, it should be taken  
 75 into account that in confined masonry construction, these elements are not designed to  
 act as moment-resisting frames. As a result, detailing of reinforcement is simple [19].  
 In fact, a common practice in Peruvian Constructions is to use corrugated steel rods of  
 $\phi 1/2''$  as longitudinal reinforcement and  $\phi 1/4''$  as transverse stirrups. Fig. 1 shows the  
 dimensions and reinforcing detail for a typical tested wall.

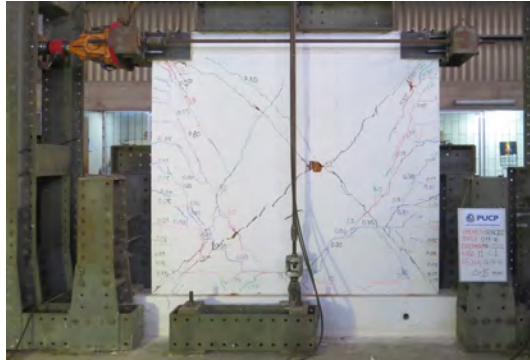
80 Regarding the experiments, in order to obtain reliable outcomes regarding the en-  
 ergy dissipation, strength and stiffness degradation of masonry walls, the cyclic char-

acter of seismic loads should be evaluated. Alternatively, the experiments could be conducted by using a shaking table where any characteristic seismic signal register can be imposed, otherwise, a cyclic test where incremental lateral displacements are imposed slowly can be used as it was demonstrated by the various experimental studies  
85 conducted by [20].

Regarding the tests conducted by [16, 17], three walls were tested under only lateral loads, until a repairable limit state was reached, i.e. equivalent to a drift of 0.125% according to the Peruvian Code [18]. The next three, unlike the previous ones, were  
90 tested until a collapsed state was reached, which had a drift of 0.833%. Finally, the last three had a constant vertical load of 170 kN, which represents the vertical load on a first floor wall from a total of three, and were tested also until reaching a collapsed state, with an associated drift of 0.625%. In this research, a total of three cracked walls were selected from the previous research to be repaired and tested under lateral cyclic loads  
95 again. Within this selection, two walls were selected from the group of walls which were led up to a collapse state (drift = 0.833%), whereas the last one was selected from the group of walls which were tested with a vertical load. It should pointed out that the walls were randomly selected for representing any cracked wall which could be located at the first floor of a masonry building.

## 100 2.2. *Characterization of the materials*

In order to characterize the properties of the materials involved in the walls, control tests were carried out at the PUCP [16, 17]. To characterize the mortar employed for the masonry panel, 12 cubic samples with dimensions 50 x 50 x 50 mm were extracted and tested under uni-axial compression. To assess the compressive behaviour and elastic  
105 modulus of the masonry, 4 masonry prisms with dimensions 230 x 130 x 600 mm were made and tested under uni-axial compression parallel to the largest dimension. In the case of a tensile behaviour of the masonry, 4 masonry walls with dimensions of 600 x 600 x 130 mm were made and tested under uni-axial compression parallel to the diagonal of each square sample (diagonal compression test). The concrete compressive  
110 strength of the foundation and confining elements was evaluated through compression tests of cylindrical specimens 150 mm wide and 300 mm high. For this job, 4 samples



(a) With vertical load W-01



(b) without vertical load W-02



(c) without vertical load W-03

Figure 2: Selected walls for retrofitting

were extracted from each concrete element. All specimens were properly cured for 28 days before testing. Table 1 shows the average results obtained from this control campaign. It is worth commenting that the concrete tensile strength and Young's modulus were computed in accordance with the CEB-FIP model code [21].

Table 1: Material properties involved in the walls

Material	Compressive strength [MPa]	Tensile strength [MPa]	Elastic modulus [MPa]
Mortar	17.50	-	-
Concrete foundation	27.50	2.18	25900
Concrete columns	19.00	1.49	22500
Concrete beam	28.00	2.22	26200
Masonry	10.00	1.40	5700

### 3. Steel Reinforced Grout (SRG)

In case of multi-storey confined masonry buildings, past earthquakes and findings of experimental studies have demonstrated the critical demand of lateral forces induced to the ground floor level, which cause significant shear cracking, and which in turn may caused the collapse of the building due to a soft story effect [22]. For this reason, in this paper, the performance of the confined masonry walls under lateral loads is intended to be improved by means of a novel retrofitting technique called SRG.

SRG is composed of ultra-high tensile strength steel fibers 100 mm wide, 0.084 mm thick, and a natural lime mortar 100 mm wide and 10 mm thick. These fibers are uni-directional since they result from twisting two wires around three straight wires. However, they are connected by perpendicular glass fiber filaments, therefore they can also be considered as textiles. As a previous step, the steel wires were coated with zinc before twisting, to protect them against corrosion [23]. The natural lime mortar employed had a M15 resistance class according to EN 998-2 and R1 according to EN 1504-3, as technical specification [24]. Furthermore, it is highly breathable, it is made strictly from natural and recycled minerals, and its manufacture produces very

low emissions of CO<sub>2</sub> and other volatile organic substances. All these properties make it part of the innovative *GreenBuilding* technology.

### 3.1. Control tests

135 In order to characterize the material properties involved in SRG, control tests were carried out. For instance, to characterize the natural lime mortar which serve as a binder for the steel galvanized fiber, 6 samples of 50 x 50 x 50 mm were made and tested after 28 days of curing, under uni-axial compression (Fig. 3a). Table 2 shows the experimental results from these tests, where the length and width resulted from  
140 averaging parallel dimensions from the face subjected to an axial load.

In the case of the galvanized steel fiber, 5 samples comprised of steel textile and steel plates which were joined by an epoxy resin, were made and tested, once the epoxy resin was totally dry (after 1 day), under uni-axial tension (Fig. 3b). In these tests, two main failure modes were recognized: one was related to the failure at the  
145 union between the textile and steel plates (U), whereas the other one was related to the middle part of the textile (M). It is worth noting that in these tests, the second failure mode is expected, in order to obtain a representative strength of the textile, since the first mode is linked to the participation of the steel plates in the failure. Table 3 shows the experimental results related to these tests, where  $E_f$  is the Young's modulus,  $f_f$  is  
150 the maximum strength, and  $\epsilon_{fu}$  is the maximum strain of the steel mesh.

Finally, the interaction between SRG and masonry substrate under shear loads was explored through 5 debonding tests, as shown in Fig. 3c, which were carried out after 28 days of curing. In these tests, 5 main failure modes were recognized: (1) rupture of the masonry substrate (2) debonding at the mortar-to-substrate interface, (3) debonding  
155 at the textile-to-mortar interface, (4) premature cracking of the outer mortar layer, and (5) rupture of the textile. Table 4 shows the experimental results related to these tests, where  $f_b$  is the maximum tensile stress developed by the steel mesh,  $\tau$  is the stress computed as the relation between the maximum force and the cross sectional area of the SRG, and  $Slip$  is the relative displacement of the SRG prior to total failure. For  
160 computing the  $Slip$ , two control points were located and connected by means of an LVDT into the specimens as is shown in Fig. 3. This LVDT measured a relative



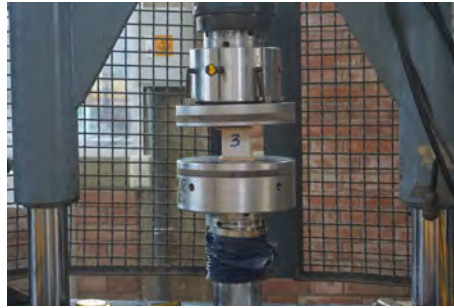
displacement,  $\delta$ , between the two control points, which was used to compute the *Slip* by means of the difference of  $\delta$  and the elastic deformation of the mesh steel,  $Slip = \delta - \epsilon_f L$ . In this expression,  $\epsilon_f$  is computed as the relation of the applied load prior total failure of the SRG,  $P$ , and the cross area of the steel mesh,  $A_f$ , multiplied by the elastic modulus of the steel mesh,  $E_f$ , namely,  $\epsilon_f = P/(A_f E_s)$ . A major detail of the control tests herein discussed is presented by [25].

Table 2: Experimental results from compressive tests

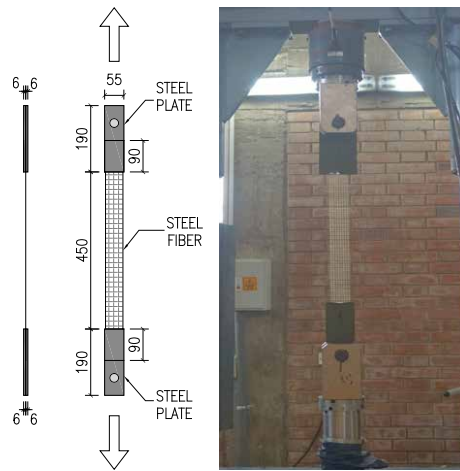
Specimen	Length [mm]	Width [mm]	Maximum Load [kN]	Stress [MPa]
M-01	50.55	50.90	57.75	22.44
M-02	51.35	50.97	60.79	23.22
M-03	51.22	50.95	58.98	22.60
M-04	51.40	51.07	62.62	23.85
M-05	51.32	50.75	57.59	22.11
M-06	51.22	50.80	60.71	23.33
Average	51.18	50.91	59.74	22.93
CV [%]	0.62	0.23	3.31	2.83

Table 3: Experimental results from tensile tests

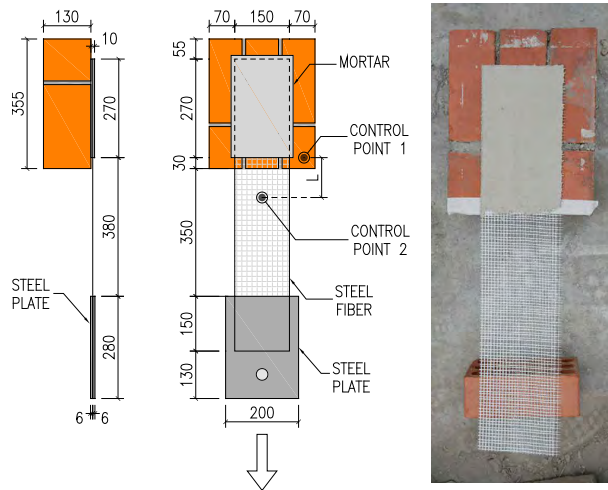
Specimen	$E_f$ [GPa]	$f_f$ [MPa]	$\epsilon_{fu}$ [%]	Failure mode
F-01	160	2786	2.18	U
F-02	161	2893	2.55	M
F-03	155	2879	2.50	M
F-04	155	2859	2.50	U
F-05	153	2886	2.45	M
Average	157	2861	2.44	-
CV [%]	2.23	1.52	6.05	-



(a) Compressive test



(b) Tensile test



(c) Debonding test

Figure 3: Testing setup for control specimens (dimensions in millimeters)

Table 4: Experimental results from debonding tests. Failure modes: (1) masonry substrate, (2) mortar-to-substrate interface, (3) textile-to-mortar interface, (4) outer mortar layer, and (5) textile

Specimen	$f_b$ [MPa]	$\tau$ [MPa]	$Slip$ [mm]	Failure mode
D-01	2068	0.66	3.50	2,4,5
D-02	1793	0.57	1.20	1
D-03	1612	0.51	2.40	3
D-04	1191	0.38	1.90	3
D-05	2023	0.64	2.20	3,4
Average	1737	0.55	2.24	-
CV [%]	20.52	20.47	37.43	-

### 3.2. Design of SRG reinforcement for shear behaviour enhancement

Before retrofitting, it is necessary to properly design the reinforcement in order to minimize the costs in materials and workmanship. For this purpose, some design concepts were extracted from the Peruvian Code, CNR-DT and AC434 [18, 14, 15], as explained below.

Regarding the adopted reinforcement scheme, CNR-DT recommends horizontal strips when a shear reinforcement is required. The nominal shear resistance of a retrofitted confined masonry wall can be evaluated as the sum of the contributions from the masonry wall and the reinforcement:

$$\phi_v V_n = \phi_v (V_m + V_f) \quad (1)$$

where  $\phi_v$  is the strength reduction factor for Load and Resistance Factor Design method (LRFD), taken as 0.75 for shear loads;  $V_m$  is the shear contribution of the masonry; and  $V_f$  is the shear contribution of the reinforcement. Regarding  $V_m$ , it should be evaluated according to local code. For instance, in this work it was evaluated according to the Peruvian Code:

$$V_m = 0.5 \cdot v'_m \cdot \alpha \cdot t \cdot L + 0.23 \cdot P_g \quad (2)$$

where  $v'_m$  is the characteristic shear strength of the masonry,  $\alpha$  is a wall slenderness factor correction,  $t$  is the wall's thickness,  $L$  is the wall's length, and  $P_g$  is the contribution of the vertical load to the shear resistance. It is worth noting that Eq. 2 refers to

the shear resistance of a new wall, therefore, an appropriate reduction factor must be employed to take into account the reduced contribution of a damaged wall.

Regarding the shear contribution of one reinforcing strip, it can be evaluated as

$$V_f = \frac{1}{\gamma} \cdot 0.6 \cdot d \cdot f_{fv} \cdot 2 \cdot \frac{A_{fv}}{p_{fv}} \quad (3)$$

where  $\gamma$  is a partial factor, taken as 1.2 for shear loads,  $d$  is the distance between the end of the fiber in compression and the centroid of the opposite confinement column,  $f_{fv}$  is the SRG design tensile strength, which can be calculated as  $f_{fv} = E_f \varepsilon_{fv}$ ,  $E_f$  is the tensile modulus of elasticity of the cracked SRG,  $\varepsilon_{fv}$  is the SRG tensile design strain, which can be taken equal to the ultimate strain of steel textile but not greater than 0.004,  $\varepsilon_{fv} = \varepsilon_{fu} \leq 0.004$ ,  $A_{fv}$  is the area of one steel textile branch, and  $p_{fv}$  is the separation between strips. Finally, the amount of strips required can be calculated as

$$n = \frac{1}{V_f} \left( \frac{V_u}{\phi_v} - V_m \right) \quad (4)$$

In the present work, for design purposes,  $V_u$  was considered as the maximum shear strength recorded by the hysteretic curves, which meant to assume that the SRG was able to recover the maximum strength in conjunction with the contribution of the repaired walls. According to Peruvian Code [18],  $V_m$  is a theoretical value which represent the shear force needed in the wall to produce the first shear crack in the masonry panel. In case of the original walls,  $V_m$  was computed using Eq. 2 as 250 kN and 211 kN for the walls with and without vertical load, respectively. However, taking into account that not all the cracks were repaired but only some of them, it was necessary to consider that the shear contribution of masonry would be a reduce part of  $V_m$ . Initially, 75% $V_m$  was taken as the shear contribution of the repaired masonry for design purposes. Nevertheless, an additional SRG strip was provided for considering that the assume percentage of 75% could be less. Experimentally, the hysteretic behaviour of the walls and what was observed during their tests showed that the lateral force which produced the first shear crack in the masonry panel of the retrofitted walls was approximately 50% of that recorded by the original walls. Therefore, for design purposes, an average value of 50% $V_m$  could be considered as adequate for the shear contribution of the repaired masonry, where  $V_m$  is computed with the Eq. 2.

195 From the geometry of a typical tested wall (Fig. 1), it was possible to deduce  
 $d = 2500$  mm. Regarding SRG's properties, it was assumed that once the SRG is  
 cracked, the tensile behaviour of the composite is governed by the steel textile. For this  
 reason,  $E_f$  was taken to be the Young's modulus of the steel mesh:  $E_f = 150$  GPa (Ta-  
 ble 3). Due to the fact that  $\epsilon_{fu}$  was greater than 0.004 in all tests (Table 3),  $\epsilon_{fv} = 0.004$   
 200 was adopted. Regarding  $A_{fv}$ , it was assumed that the strips were 100 mm wide and that  
 there were 16 steel cords, which resulted in  $A_{fv} = 8.6$  mm<sup>2</sup> according to the manufac-  
 turer's data sheet [23]. Finally, 450 mm was assumed as the separation between strips  
 for design purposes. Fig. 4 shows the reinforcing scheme adopted for the present work.

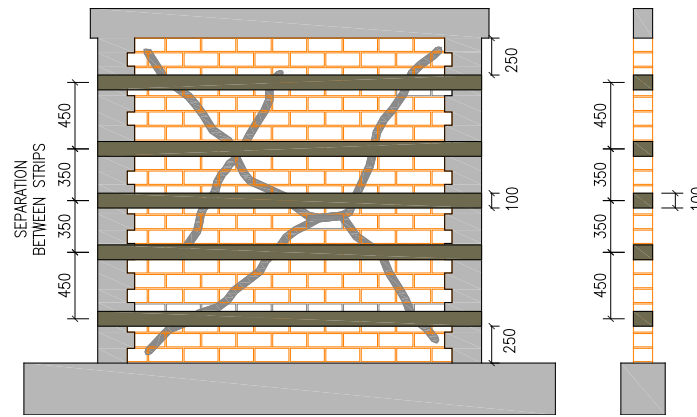


Figure 4: Details of the reinforcement for the repaired walls (dimensions in millimeters)

It should be noted that in Fig. 4, less separation between the strips was assumed  
 205 at the mid-height of the walls. This assumption was related to the fact that the largest  
 number of cracks were concentrated in the mid-height of the walls.

### 3.3. Procedure for retrofitting confined masonry walls with SRG

Before retrofitting, it is necessary to make a proper repair of the cracks since a good  
 repair improves the recovery of the initial stiffness. In this study, cracks greater than 8  
 210 mm were opened using hand tools in order to avoid excessive out-of-plane effects. In  
 the case of crushed bricks, it is recommended to replace them by new ones (Fig. 5b).  
 Thereafter, the openings were filled with reparation mortar based on Portland cement  
 with a volumetric ratio cement/sand = 1/3. After being repaired, the walls should be

properly cured for at least 28 days. However, taking into account what would be done  
215 in a massive application, they were moistened three times a day for seven days. In this  
way, it was hoped to guarantee a reasonable resistance of the reparation mortar. Fig. 5  
shows the main steps involved in repairing CMW.



(a) Cracks opening



(b) Filling of openings



(c) Curing process

Figure 5: Main steps for repairing CMW (W-01)

Regarding retrofitting, there are two previous jobs needed for the proper prepara-  
220 tion of the zone of intervention. The first one is related to the fact that additional  
roughness can be provided by punching the bricks lightly by means of pointed tools.  
The second one consists in delimiting the intervention zone by means of Scotch tape.  
Although these jobs are not obligatory, they allow providing better adhesion between  
the SRG and the masonry substrate, as well as saving on material by using only what  
is necessary.

225 The retrofitting process started by moistening the intervention zone in order to avoid  
the absorption of the SRG's water by the masonry. Then, a first layer of mortar, 5  
mm thick, was laid upon the masonry within the area delimited by the Scotch tape.  
Subsequently, the steel mesh was embedded lightly inside the first layer of mortar.  
Thereafter, a second layer of mortar 5 mm thick was laid in order to finish covering the  
230 embedded steel mesh. Finally, once all the SRG strips were finished, the Scotch tape  
was removed to start the curing process. Fig. 6 shows the main stages of the retrofitting  
process as explained above. It is worth noting that, in this work, it was possible to  
anchor the steel mesh by overlapping them 250 mm interspersed at each column's  
ending, because it only had to reinforce isolated walls. However, for other applications,  
235 a proper anchor for the steel mesh must be previously studied or applied according to  
the manufacturer's recommendations, in order to guarantee a good transmission of the  
stresses from the masonry to the SRG. Like reparation mortar, an SRG composite needs  
a proper curing process of at least 28 days. However, again taking into account what  
would be done in a massive application, the SRG composite was moistened for 14 days  
240 to guarantee a good mortar strength before testing.

#### *3.4. Boundary conditions and instrumentation for the cyclic tests*

Before testing, each foundation end was fixed to a reaction slab by means of hy-  
draulic jacks to restrict them vertically. Another hydraulic jack and a reaction frame  
were used as rigid horizontal stops also for the foundation ends. A vertical load of  
245 170 kN was applied by another hydraulic jack through two rigid steel beams in order  
to distribute the vertical load along the confinement beam. Regarding the horizontal  
cyclic loads, they were applied at the top of the wall by means of a dynamic actuator  
which was controlled by a computer.

Regarding the instrumentation, linear variable differential transformers (LVDTs)  
250 were placed, as shown in Fig. 7. Two LVDTs (LVDT 1 and 2) were placed along  
the diagonals of the masonry panel to measure their deformations and thus to have  
enough data in case an idealized strut-and-tie model is carried out. Another two LVDTs  
(LVDT 3 and 4) were placed at the confinement columns to measure their deformations  
due to vertical loads and bending effects during the cyclic test. One LVDT (LVDT 5)



(a) First layer of mortar



(b) Placement of steel fiber mesh



(c) Second layer of mortar



(d) Retrofitted wall

Figure 6: Stages for strengthening CMW with SRG (W-02)



255 was placed between the geometric centre of the confining beam and a reaction frame, which was assumed to be static. Fig. 7 shows the general testing setup as well as the instrumentation scheme for each cyclic test.

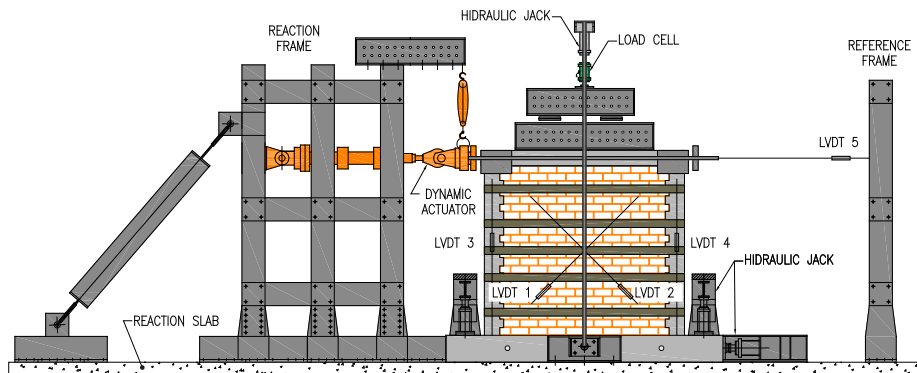


Figure 7: Setup and instrumentation for cycling test

The cyclic loading was controlled by displacements, which means that the dynamic actuators applied displacements instead of forces. However, this had an internal load cell that allowed registering the load related to each displacement, thus it was possible to plot the corresponding hysteretic behaviour. In order to avoid kinematic effects, a quasi-static test was intended to be carried out by applying an average velocity of 0.25 cycles/minute. Regarding the applied history of displacements, it was defined according to FEMA 461 [26]. Thereby, each level of displacement resulted from increasing the previous level of displacement by a factor of 1.4. In addition, two cycles were also defined for each displacement level. It is worth highlighting that in the previous work [16, 17], only 11 displacement phases were considered, with a maximum displacement level of 20 mm, whereas in this work, 12 displacement phases have been taken into account, with a maximum displacement level of 30 mm, as shown in Fig. 8.

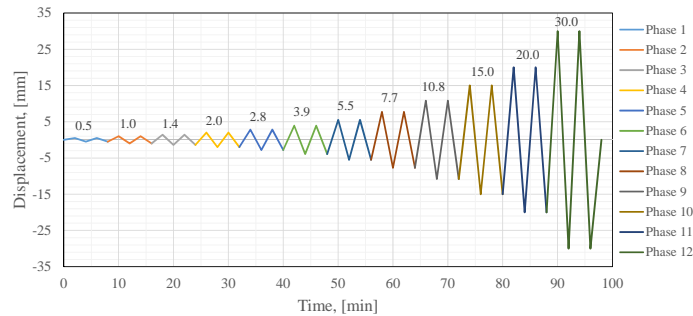


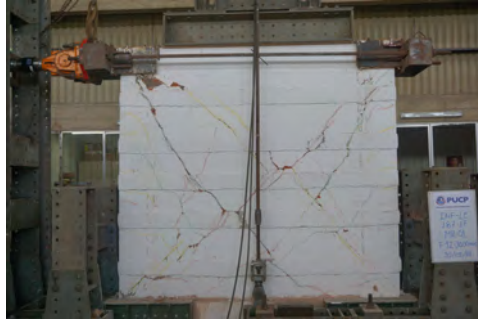
Figure 8: History of displacements

## 270 4. Discussion of the results

### 4.1. Cracking pattern

Within the category of confined masonry buildings, masonry walls act as bearing elements. Therefore, a premature failure of these walls would result in the building's collapse. In performance design, it is intended that the building has a specific performance level, which in turn is related to the post-earthquake disposition of the building. 275 These performance levels can be roughly classified and assigned to certain levels of drift: (1) Immediate Occupancy (IO) – drift = 0.3%, (2) Life Safety (LS) – drift = 0.6%, and (3) Collapse Prevention (CP) – drift = 1.0%, as it was established by FEMA 356 after evaluating a huge quantity of experimental studies referred to masonry walls 280 [27]. Fig. 9 shows the final cracking pattern for all the tested walls, whereas Table 6 shows the evolution of cracking according to each performance level.

In general, all the retrofitted walls showed bending cracks at the columns' feet prior to a drift of 0.12%, which corresponds to the fifth loading phase. Subsequently, the cracks that were previously repaired started opening. However, it should be noted that 285 not only the repaired cracks were opened during the tests, on the contrary, additional cracks took place. This effect can be noted in Table 6 by comparing the cracking pattern of retrofitted walls with those un-retrofitted. In addition, it is worth also noting that the tested walls suffered a mixed failure mode, namely, they started having cracks due to bending effects but finished having cracks also due to shear effects.



(a) RW-01



(b) RW-02



(c) RW-03

Figure 9: Cracking pattern of tested walls

290 Concerning the in-plane seismic behavior of the confined masonry walls, initially, the masonry panel resists by itself all the effects caused by the lateral forces, whereas the confining elements do not play a significant role. Nevertheless, once the masonry panel is cracked, the vertical reinforcement in confining columns start engaging in resisting tension and compression stresses [19]. This fact explained why and how con-  
295 fining elements play an important role into the lateral displacement ductility capacity of the confined masonry walls. Therefore, it is also important to assess the cracking evolution of these elements.

#### 4.1.1. RW-01

During the fifth loading phase (drift = 0.12%), the first visible cracks occurred at the  
300 columns' feet because of bending effects. Thereafter, progressive bending cracks began to appear along the column's height. These cracks were produced by the controlled elongation of the confining columns, given by the bond-slip effect present in the RC frames, during each loading phase [28]. It should be taken into account that whereas the steel reinforcement is able to carry tensile stresses, the concrete and masonry are  
305 able to carry compressive stresses and the wall is still stable, the confining frames will provide lateral displacement ductility to the wall. By comparing the reinforced wall with the original one, even when the cracks in the columns were not repaired, it could be observed that no extra cracks were significantly produced in these elements (Table 6). This is related to the fact that during the test, the confining elements acted as  
310 cracked elements, therefore, the cracks opened during the test were almost the same as those that were not repaired.

Regarding the masonry panel, the first diagonal crack produced by shear effects took place at the seventh loading phase (drift = 0.23%). It should be noted that as the displacements increased, additional cracks due to shear effects occurred. Instead of  
315 RW-02 and 03, in this wall it was possible to observe the rupture of two SRG strips at the mid-height of the wall, which demonstrated that all the strength of the SRG could be developed. Nevertheless, it is worth mentioning that the ruptures were characterized by the breakage of the steel meshes and not by debonding failure, which demonstrated a perfect adhesion among the SRG's mortar and masonry substrate. Similarly, other

320 SRG strips showed elongations of the steel mesh, which could be observed because of  
the detachment of the external layer of the mortar.

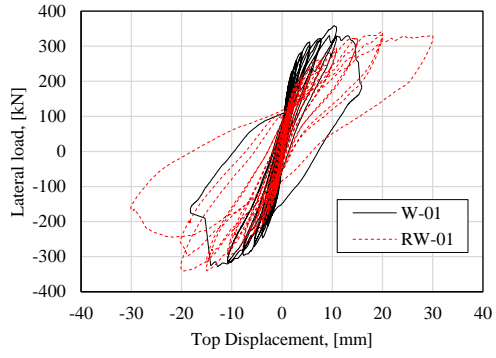
#### 4.1.2. RW-02 & RW-03

Like RW-01, the first visible cracks in these walls occurred at the columns' feet due  
to bending effects. However, unlike RW-01, they took place at the fourth loading phase  
325 (drift = 0.083%). With respect to the cracking of the confining columns, like RW-  
01, as the displacements increased, the number of cracks in height increased as well.  
Furthermore, it could also be noted that no extra cracks were significantly produced in  
the confining columns (Table 6).

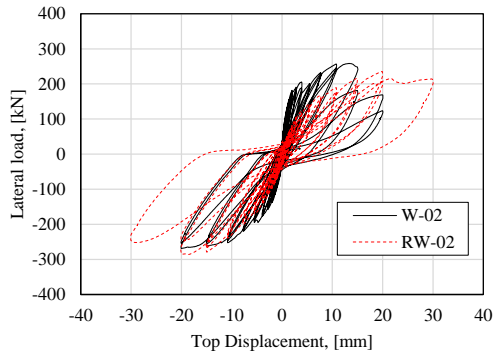
Regarding the masonry panel, the first diagonal crack produced by shear effects  
330 took place at the eleventh (drift = 0.833%) and ninth (drift = 0.45%) loading phase,  
respectively. In addition, it should be noted that as the displacements increased, addi-  
tional cracks due to shear effects took place. Unfortunately, in these walls it was not  
possible to develop the total tensile strength of the SRG strips. Nevertheless, it should  
be highlighted that this means they were prepared to withstand more tensile stress than  
335 they were subjected to. In addition, it is worth noting that a horizontal crack took place  
in both cases at the base of the wall, to have a sort of rocking effect, as is shown by the  
shape of the hysteresis loops in Fig. 10. The results associated to the first cracking and  
maximum load capacity are summarized in Table 5.

In all cases, the collapse state was governed by the instability of the walls or the  
340 abrupt loss in load capacity either within the first or second hysteresis loop of the  
corresponding loading phase. For instance, Fig. 10 (a) and (b) show only one cycle  
in the last loading phase, which was associated to the instability of the walls, whereas  
Fig. 10 (c) shows an abrupt loading loss in the second cycle of the last loading phase.

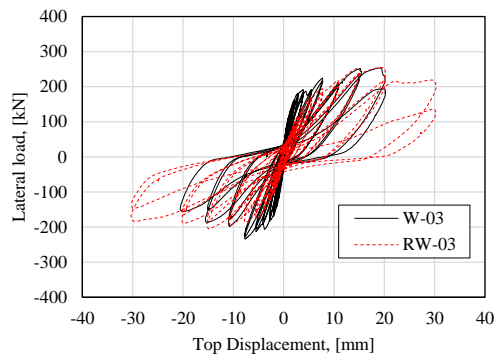
Regarding the performance of the retrofitted walls, it is worth highlighting that  
345 only the retrofitted walls managed to prevent a collapse. Namely, the original walls  
were not able to withstand the drift level associated with collapse prevention (drift =  
1.00%), whereas once repaired and retrofitted with SRG they were able to attain that  
level of performance (Fig. 11). In fact, this helps to reduce the risk of life-threatening  
injury, which is of great interest in seismic areas.



(a)

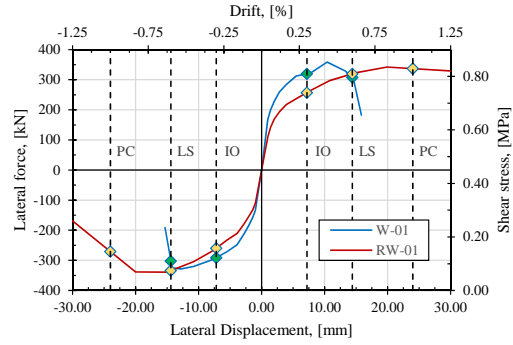


(b)

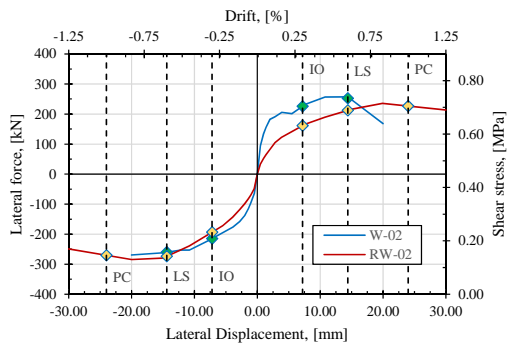


(c)

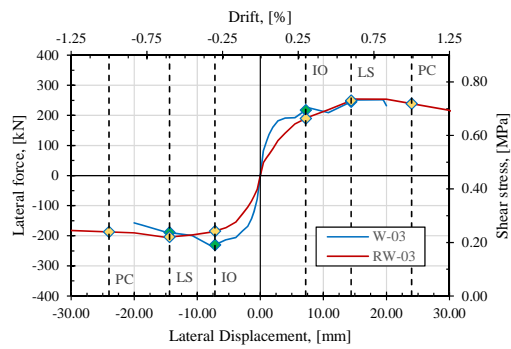
Figure 10: Hysteresis curves of tested walls



(a)



(b)



(c)

Figure 11: Envelope curves of tested walls

Table 5: Experimental results of tested walls

Specimen	Direction	First cracking		Maximum load	
		Load [kN]	Drift [%]	Load [kN]	Drift [%]
RW-01	Push	195	0.116	340	0.833
	Pull	-180	-0.116	-340	-0.833
RW-02	Push	90	0.083	235	0.833
	Pull	-120	-0.116	-285	-0.833
RW-03	Push	95	0.083	255	0.625
	Pull	-125	-0.116	-205	-0.625

#### 350 4.2. Lateral displacement ductility

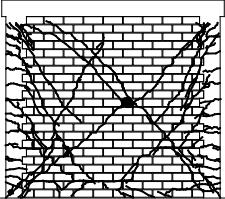
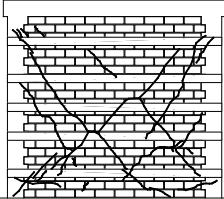
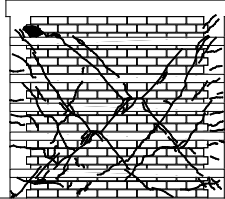
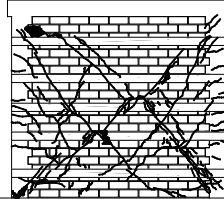
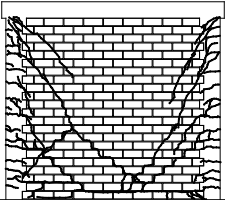
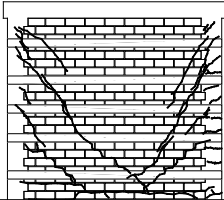
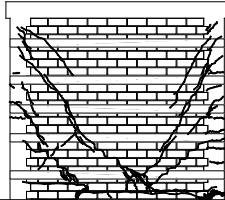
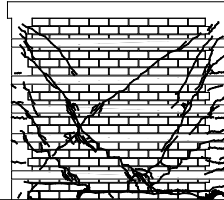
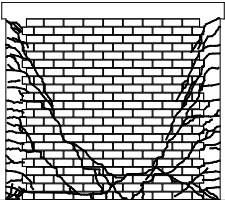
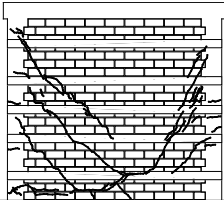
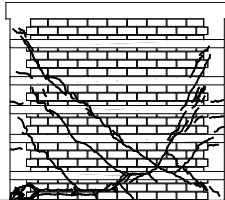
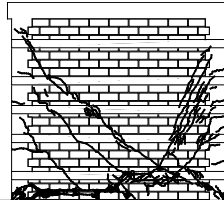
As mentioned above, the original walls were not able to reach the performance level of collapse prevention, which means they did not have enough ductility to resist lateral forces while maintaining their stability. Taking into account the final lateral displacement reached by each wall,  $\delta_u$ , and the displacement related to the first cracking of the masonry panel,  $\delta_y$ , the ductility was evaluated according to Eq. 5. In order to evaluate  $\delta_y$ , backbone curves were traced from the envelope curves shown in Fig. 11, by following the recommendations of [29]. These backbone curves were drawn by highlighting three main point: (1) first cracking, (2) maximum strength, and (3) ultimate state, as is shown in Fig. 12.

$$\mu = \frac{\delta_u}{\delta_y} \quad (5)$$

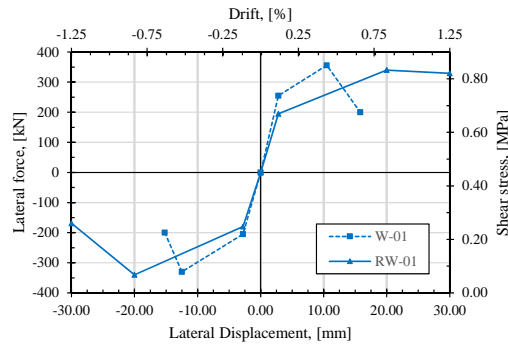
360 Table 7 shows a summary of the calculation of the ductility developed for each tested wall. It has to be noted that in the case of RW-01 the increment in ductility was about 100%, whereas in the rest it was about 50%. It also has to be pointed out that the original walls withstood higher forces than the retrofitted ones in the first performance level (IO), as can be seen in Fig. 11. However, for the second performance level   
365 (LS), both the original and retrofitted walls showed almost the same strength. Finally, the retrofitted walls, besides being the only ones which could reach the last desired performance level (PC), were able to withstand almost the same level of lateral forces



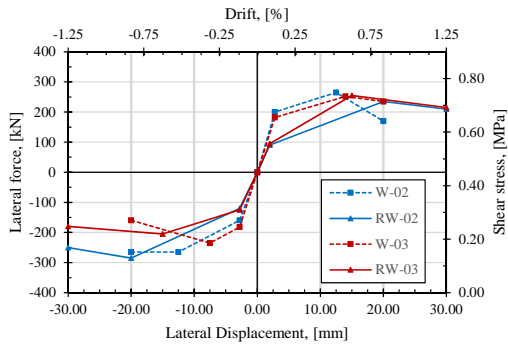
Table 6: Cracking evolution of tested walls

 <p>(a) Final state [W-01]</p>	 <p>(b) IO [RW-01]</p>	 <p>(c) LS [RW-01]</p>	 <p>(d) CP [RW-01]</p>
 <p>(e) Final state [W-02]</p>	 <p>(f) IO [RW-02]</p>	 <p>(g) LS [RW-02]</p>	 <p>(h) CP [RW-02]</p>
 <p>(i) Final state [W-03]</p>	 <p>(j) IO [RW-03]</p>	 <p>(k) LS [RW-03]</p>	 <p>(l) CP [RW-03]</p>

as the LS. This means that after the LS performance level, the retrofitted walls could continue withstanding forces by maintaining their stability.



(a) with vertical load



(b) without vertical load

Figure 12: Backbone curves of tested walls

370 **4.3. Energy dissipation and damping ratio**

The Ultimate Limit State (ULS) design approach considers the maximum strength that could be withstood by the structural elements. This is considering both linear and non-linear behaviour of the elements, either due to material or geometric non-linearity. Whenever non-linear behaviour takes place, inelastic strains are experienced, which  
 375 produce damage in the structural elements. It should be noted that the more inelastic strains there are, the more structural damage will take place. During this process, a

Table 7: Improved ductility calculation of tested walls

Specimen	$\delta_y$	W		RW		Increment
		$\delta_u$ [mm]	$\mu$	$\delta_u$ [mm]	$\mu$	
01	2.8	15.0	5.35	30.0	10.7	100
02	2.8	20.0	7.14	30.0	10.7	50
03	2.8	20.0	7.14	30.0	10.7	50

certain amount of energy absorption and dissipation is involved. In this section, the energy dissipation,  $E_d$ , will be evaluated by the area within each hysteretic loop, as shown in Fig. 13. Additionally, the equivalent hysteretic viscous damping,  $\xi_{hyst}$ , is evaluated as the ratio between the dissipated energy and the elastic strain energy, as shown in Fig. 13.

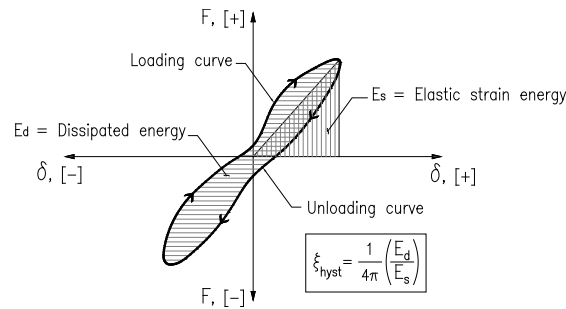


Figure 13: Calculation of energy dissipation and damping ratio

Fig. 14 shows the cumulative energy dissipated for each loading phase. It has to be noted that the SRG gave the original walls the ability to dissipate more energy by means of greater inelastic displacements. In general terms, both the original and retrofitted walls had almost the same cumulative energy dissipation until the maximum displacement of the original walls. However, a freak tendency could be observed in the last loading phase of W-01, where an abrupt increment of energy dissipated was captured, as is shown in Fig. 14. This is related to the fact that in this loading phase an abrupt loss of capacity load (Fig. 10a) was registered, which in turn resulted in a quite large hysteretic loop. A similar phenomenon was registered for RW-01. However, this took place for a displacement that corresponded to the double of its original wall and

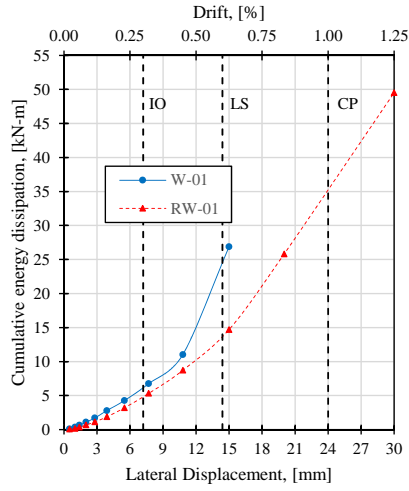
this occurred only in the pulling branch of the hysteresis loop (Fig. 10a).

During the cyclic tests, it was possible to note that there were areas enclosed by the loops of the first two loading phases when they were expected to have no areas for corresponding to a linear-elastic behaviour. This anomalous behaviour was related to the fact that, like any mechanical equipment, the dynamic actuator needed certain small displacements for being calibrated. Therefore, to take into account this assumption, the first two loading phases were excluded from the calculation of the average hysteresis damping. Fig. 15 shows the variation of the hysteresis damping along the incremental loading phases for each tested wall. It is worth noting that the retrofitted walls had greater values of hysteresis damping throughout the tests. Nevertheless, the freak energy dissipation just mentioned also affected the calculation of the hysteresis damping in the last loading phase of W-01. For this reason, this value was also excluded from the computation of the average hysteresis damping. Once this assumption is made, it is possible to note that RW-01 showed an average hysteresis damping of 9.65% against the 7.90% of W-01, which means an increment of 20%. RW-02 showed an average hysteresis damping of 12.00% against the 10.50% of W-02, which means an increment of 14%. Finally, RW-03 showed an average hysteresis damping of 12.45% against the 9.90% of W-03, which mean an increment of 26%.

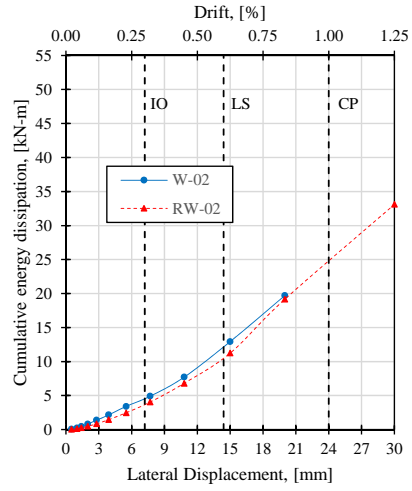
#### 4.4. Initial stiffness and stiffness degradation

Fig. 16 shows the stiffness degradation of the tested walls. The same effect of the first two hysteresis loops is shown when computing the initial stiffness. Therefore, the initial stiffness was considered as that related to the third loop. It is important to highlight that the recovery of the initial stiffness will be as good as the goodness of the repair. On the other hand, since one aim of this work is to show that repairing and retrofitting with SRG can be done in an easy and massive way, this work tried to reproduce an effective and economic repair job, as explained above. This resulted in a recovery of 75% of the original wall's initial stiffness for RW-01 and 50% for RW-02 and 03.

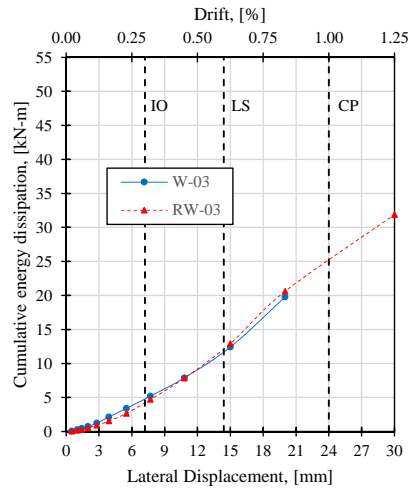
Regarding stiffness degradation, it is known that it can be the result of cracking, crushing, rebar buckling, cracks opening and closing, among other factors. Likewise,



(a)

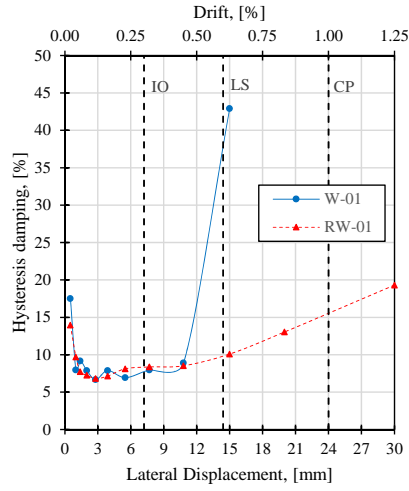


(b)

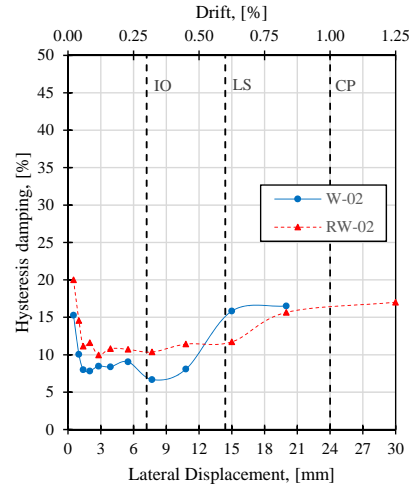


(c)

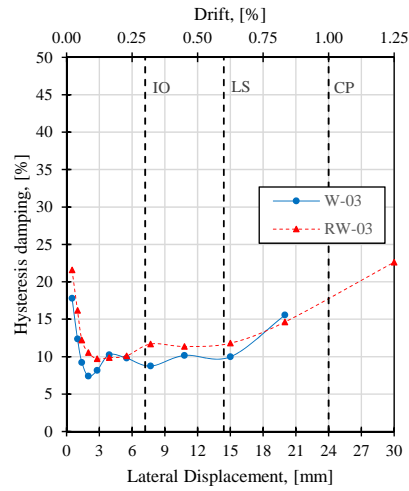
Figure 14: Cumulative energy dissipation for tested walls



(a)

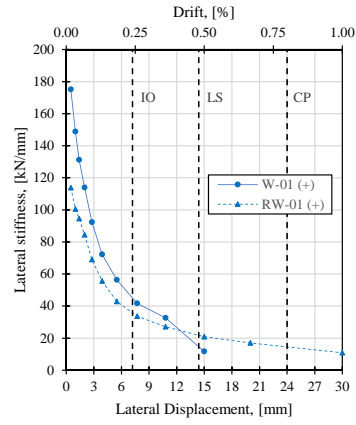


(b)

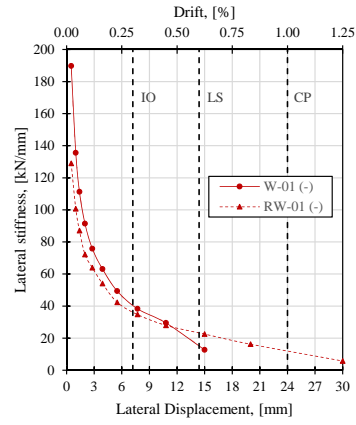


(c)

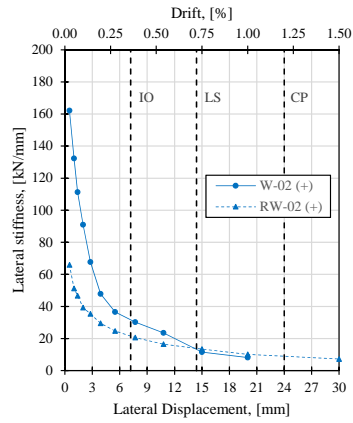
Figure 15: Hysteretic damping ratio for tested walls



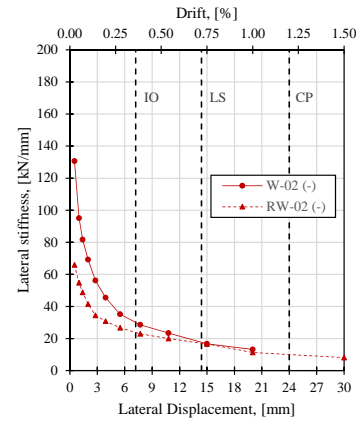
(a)



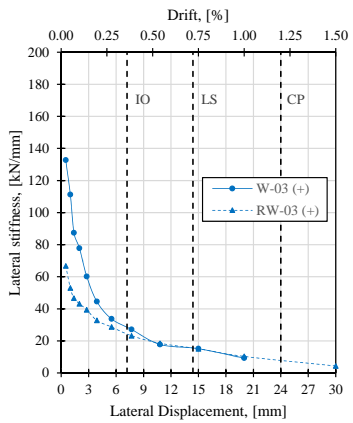
(b)



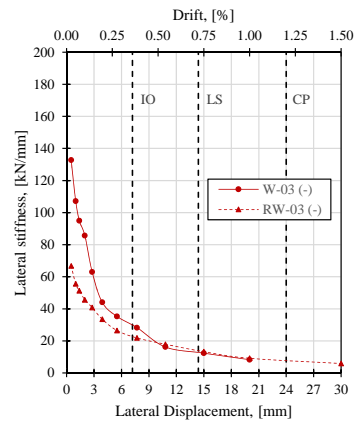
(c)



(d)



(e)



(f)

Figure 16: Stiffness degradation for tested walls

the level of stiffness degradation is related to the features of the structure (e.g. material properties, geometry, connection types), as well as to the loading history (e.g. displacement level for each loading phase, number of cycles per phase, increment ratio of displacements) [30]. The stiffness degradation is very helpful for design codes since it allows them to define the drifts according to the expected performance levels. In this case, following the three main desired performance levels (IO, LS and CP), the stiffness decay of the initial stiffness of the retrofitted walls was evaluated for each of these states, as described in Table 8.

Table 8: Percentages of stiffness at performance levels regarding initial stiffness

Wall	Immediate Occupancy (IO)	Life Safety (LS)	Collapse Prevention (CP)
W-01	35%	12%	-
RW-01	40%	25%	15%
W-02	32%	16%	-
RW-02	47%	32%	20%
W-03	32%	16%	-
RW-03	48%	30%	16%

The vertical load applied to W/RW-01 gives them more stiffness which is clearly evidenced in the first loading phases. However, at the same time, this makes them more brittle, which means they lose stiffness more quickly than W/RW-02 and 03, as new cracks take place or existing cracks become enlarged. Moreover, taking into account the fact that before the retrofitting, the walls were totally failed, one can be sure that the SRG had an impact on reducing the brittle behaviour of confined masonry walls. Indeed, Fig. 16 shows that regardless of the walls, the retrofitted ones showed a lesser stiffness degradation than the original walls, which in turn was related to the stability of the walls.

## 5. Conclusions

The suitability of SRG as a seismic retrofitting technique was evaluated by applying it externally to three confined masonry walls and testing them under cyclic in-plane



loads. Prior to the retrofitting, the walls were subjected to cyclic loads and were led to their ultimate limit state. It should be noted that of the three tested walls, one had a vertical load of 170 kN during the testing and the rest were only subjected to lateral loads.

A design procedure was developed by taking some concepts from the Peruvian Code, CNR-DT and AC434. Subsequently, the retrofitting system consisted of 5 SRG strips, each one with a thickness of 10 mm and a width of 100 mm. Within each strip, there was embedded a mesh of 0.084-mm thick galvanized steel fiber. The retrofitting process was also given in detail, showing its easy maneuverability and applicability of the materials involved.

The experimental results showed that there was a considerable improvement of the seismic performance of the retrofitted confined masonry walls in comparison with the original ones. In terms of ductility, SRG showed a substantial increment of the lateral deformation capacity by 100% in one wall and 50% in the rest. Parallel to the improvement in ductility, it should be highlighted that the retrofitted walls were able to perform correctly even after the performance level of collapse prevention (drift=1%) while maintaining their stability. In terms of energy dissipation, the retrofitted walls showed they were able to dissipated more energy than the original walls. Likewise, greater average values of hysteresis viscous damping were registered during the incremental loading phases. Finally, taking into account that the retrofitting was applied to failed walls, it was possible to observe that the SRG allowed the walls to enjoy a slighter degradation of their stiffness than the original walls. In this way, the brittle behaviour was improved and also the integrity and stability of the walls were guaranteed.

#### **Acknowledgment**

The authors are grateful for the financial support provided by CONCYTEC within the framework of the N° 232-2015-FONDECYT Agreement, as well as to the industrial company KERAKOLL for providing the necessary materials for the retrofitting.

## References

- 470 [1] INEI, Censos nacionales 2014: población y vivienda, Instituto nacional de estadística e informática.
- [2] N. Kassem, A. Atta, E. Etman, Structural Behavior of Strengthening Masonry In-filled Frames Subjected to Lateral Load using Bonded and Un-bonded CFRP, *KSCE Journal of Civil Engineering* 21 (3) (2016) 818–828.
- 475 [3] M. El-Diasity, H. Okail, O. Kamal, M. Said, Structural performance of confined masonry walls retrofitted using ferrocement and GFRP under in-plane cyclic loading (2015) 54–69.
- [4] B. Ozsayin, E. Yilmaz, M. Ispir, H. Ozkaynak, E. Yuksel, A. Ilki, Characteristics of CFRP retrofitted hollow brick infill walls of reinforced concrete frames, *Construction and Building Materials* 25 (10) (2011) 4017–4024.
- 480 [5] E. Quagliarini, F. Monni, F. Greco, S. Lenci, Flexible repointing of historical facing-masonry column-type specimens with basalt fibers: A first insight, *Journal of Cultural Heritage*.
- [6] N. Gattesco, I. Boem, Characterization tests of GFRM coating as a strengthening technique for masonry buildings, *Composite Structures* 165 (2017) 209–222.
- 485 [7] T. C. Triantafillou, C. G. Papanicolaou, Textile Reinforced Mortars (TRM) versus Fiber Reinforced Polymers (FRP) as Strengthening Materials of Concrete Structures, *Special Publication* 230 (2005) 99–118.
- [8] C. G. Papanicolaou, T. C. Triantafillou, M. Papathanasiou, K. Karlos, Textile reinforced mortar (TRM) versus FRP as strengthening material of URM walls: out-of-plane cyclic loading, *Materials and structures* 41 (1) (2008) 143–157.
- 490 [9] A. Razavizadeh, B. Ghiassi, D. V. Oliveira, Bond behavior of SRG-strengthened masonry units: Testing and numerical modeling, *Construction and Building Materials* 64 (2014) 387–397.

- 495 [10] A. Borri, P. Casadei, G. Castori, J. Hammond, Strengthening of brick masonry arches with externally bonded steel reinforced composites, *Journal of composites for construction* 13 (6) (2009) 468–475.
- [11] E. Wobbe, P. Silva, B. Barton, L. Dharani, V. Birman, A. Nanni, T. Alkhrdaji, J. Thomas, T. Tunis, Flexural capacity of RC beams externally bonded with SRP and SRG, in: *Proceedings of Society for the Advancement of material and Process Engineering 2004 Symposium*, 2004, pp. 16–20.
- 500 [12] B. Barton, E. Wobbe, L. R. Dharani, P. Silva, V. Birman, A. Nanni, T. Alkhrdaji, J. Thomas, G. Tunis, Characterization of reinforced concrete beams strengthened by steel reinforced polymer and grout (SRP and SRG) composites, *Materials Science and Engineering: A* 412 (1-2) (2005) 129–136.
- 505 [13] S. De Santis, F. Ceroni, G. De Felice, M. Fagone, B. Ghiassi, A. Kwiecie, G. Lignola, M. Morganti, M. Santandrea, M. Valluzzi, A. Viskovic, Round robin test on tensile and bond behaviour of steel reinforced grout systems, *Composites Part B*.
- [14] CNR-DT-200-R1, Guide for the design and construction of externally bonded FRP systems for strengthening existing structures, Advisory Committee on Technical Recommendations for Construction.
- 510 [15] AC-434, Acceptance criteria for masonry and concrete strengthening using Fabric-Reinforced Cementitious Matrix (FRCM) and Steel Reinforced Grout (SRG) composite systems, International Code Council - Evaluation Service.
- 515 [16] J. Manchego, S. Pari, Análisis experimental de muros de albañilería confinada en viviendas de baja altura en Lima, Perú, Master's thesis, Pontificia Universidad Católica del Perú (2016).
- [17] M. Luján, Refuerzo de muros de albañilería confinada con mallas de acero.
- [18] E070, Reglamento nacional de edificaciones: Albañilería, Ministerio de Vivienda, Construcción y Saneamiento - SENCICO.
- 520

- [19] S. Brzev, Earthquake-Resistant Confined Masonry Construction, NICEE, National Information Center of Earthquake Engineering, Indian ?, 2007.
- [20] M. Tomažević, M. Lutman, L. Petković, Seismic behavior of masonry walls: Experimental simulation, *Journal of Structural Engineering* 122 (9) (1996) 1040–1047.
- 525
- [21] CEB-FIP, Model code 2010, London: Thomas Telford.
- [22] S. Brzev, M. Astroza, O. Moroni, Performance of confined masonry buildings in the February 27, 2010 Chile earthquake, Earthquake Engineering Research Institute, Oakland, California ([www.confinedmasonry.org](http://www.confinedmasonry.org)).
- 530
- [23] Kerakoll, GeoSteel G600, Tech. rep., Kerakoll - The GreenBuilding Company (2013).
- [24] Kerakoll, GeoCalce F Antisismico, Tech. rep., Kerakoll - The GreenBuilding Company (2017).
- [25] J. Salsavilca, J. Yacila, N. Tarque, G. Camata, Experimental and analytical bond behavior of masonry strengthened with steel reinforced grout (SRG), submitted manuscript.
- 535
- [26] A. T. Council, M.-A. E. Center, M. C. for Earthquake Engineering Research (US), P. E. E. R. Center, N. E. H. R. P. (US), Interim Testing Protocols for Determining the Seismic Performance Characteristics of Structural and Nonstructural Components, Federal Emergency Management Agency, 2007.
- 540
- [27] P. FEMA, Commentary for the seismic rehabilitation of buildings, FEMA-356, Federal Emergency Management Agency, Washington, DC.
- [28] M. Dehestani, S. Mousavi, Modified steel bar model incorporating bond-slip effects for embedded element method, *Construction and Building Materials* 81 (2015) 284–290.
- 545
- [29] A. S. of Civil Engineers, Seismic evaluation and retrofit of existing buildings: *Asce/sei*, 41-17, American Society of Civil Engineers, 2017.

[30] A. T. Council, Effects of strength and stiffness degradation on seismic response, FEMA P440A.